

# Morphology of islanded transition-metal films on graphite studied by extreme-UV reflectivity

C. Binns, S. H. Baker, A. M. Keen, S. N. Mozley, and C. Norris

*Department of Physics and Astronomy, University of Leicester, Leicester LE1 7RH, United Kingdom*

H. S. Derbyshire and S. C. Bayliss

*Department of Physics, DeMontfort University, Leicester LE1 9BH, United Kingdom*

(Received 3 May 1995)

We report a study of the growth and morphology of islanded thin films of manganese, chromium, and vanadium on graphite substrates using surface reflectivity in the extreme ultraviolet region (6–36 nm). Over a large range of coverage, the reflectivity is well described by a film consisting of a continuous slab with an effective refractive index calculated for an inhomogeneous layer of identical ellipsoids. This model gives good agreement with experimental measurements for coverages up to the percolation threshold. At very low coverages, modeling the film as an array of independent spheres, the extinction of which is calculated using Mie theory, gives better results. The combination of models allows the film thickness, coverage, and average island size and shape to be determined from the earliest stages through to almost continuous films. In all cases, the metal islands are nearly spherical at intermediate coverages, becoming flattened with increasing coverage. In the case of chromium, at a substrate temperature of 423 K, the film grows as an increasing density of particles of constant size, whereas at 453 K the growth mode changes to one consisting of a roughly constant number of particles whose volume increases linearly with evaporation time. At 498 K the film consists of a large number of very small (1.2 nm) islands. The growth of vanadium at 423 K is similar to that of chromium at the same temperature. Manganese growth at 423 K is more complex showing a change in growth mode as a function of coverage.

## I. INTRODUCTION

The study of the anomalous optical properties of inhomogeneous media has a long history. It was Michael Faraday<sup>1</sup> who first speculated, correctly, that the brilliant colors observed when viewing very thin gold and silver films in white light was due to their granular nature. The same effects are seen in colloids, and the general solution to absorption and scattering of light by spherical particles was first formulated by Mie.<sup>2</sup> This theory explained the presence of anomalous absorption bands when the wavelength is of the same order of magnitude as the particle size. Likewise, the reflectivity of a deposited in homogeneous film shows features observed neither in the bulk or in a continuous layer, and is highly sensitive to the film morphology.

Jarrett and Ward<sup>3</sup> and McKenna and Ward<sup>4</sup> used visible light to study the shapes of gold and silver islands grown on glass and mica substrates. They extended the theory of Maxwell-Garnett,<sup>5</sup> based on spherical particles, to include ellipsoidal geometries and found that, in general, islands become flatter with increasing coverage. Schade and Smith<sup>6</sup> used Mie theory to determine the surface roughness of fluorinated tin oxide films, and Binns and Bayliss<sup>7</sup> used a model based on Mie theory to obtain the average size of silver islands grown by deposition on graphite. Recently measurements have been extended into the extreme ultraviolet (xuv) region of the spectrum to determine the average size of mesoscopic transition metal islands on graphite.<sup>8</sup> The reflectivity of light in the xuv region, whose wavelength is of the order of a few nanometers, is particularly sensitive to the morphology of films consisting of mesoscopic particles.

Here we report an extension of our earlier models based

on Mie theory to higher coverages using the theory of Jarrett and Ward. By comparing the measured spectral dependence of the xuv reflectivity with calculations using the two models, we have carried out a study of the growth of chromium, vanadium, and manganese on graphite, and have been able to monitor the effect of substrate temperature on the morphology of the films.

## II. EXPERIMENT

All measurements were made using the grazing incidence monochromator on beamline 6.1 of the synchrotron radiation source (SRS) at Daresbury laboratory. This provides usable light flux in the spectral range 35–200 eV (35.42–6.20 nm). The specular reflectivity of samples at a grazing angle of 22.5° was measured using an EMI nude photomultiplier assembly with CuBe dynodes.

Chromium and manganese films were deposited using Knudsen cell sources, and vanadium was evaporated from the end of a rod heated by electron bombardment. All sources were surrounded by cooling shrouds through which circulated a chilled water/antifreeze mixture. The chamber base pressure was  $2 \times 10^{-11}$  mbar, and was always less than  $2 \times 10^{-10}$  mbar during film growth, recovering within a few minutes to the base vacuum. The highly oriented pyrolytic graphite (HOPG) substrates were cleaved *ex situ* and heated to 800 °C for 30 min in the vacuum system to remove any residual gas. Photoemission measurements showed no trace of intercalated contaminants for the substrates used during the chromium and vanadium experiments. Small traces of silicon were observed on some of the substrates prior to the growth of manganese films. The spectral dependence of the

reflectivity of the clean substrates in this case was identical to those with no trace of contamination, so the silicon produces no optical effect though it may perturb the characteristics of the film growth.

The reflectivity was obtained from the reflected signal from the covered substrate,  $I(\lambda)$ , using the relation

$$R(\lambda) = \frac{I(\lambda)}{I_0(\lambda)} R_0(\lambda),$$

Where  $I_0(\lambda)$  is the signal from the clean substrate, and  $R_0(\lambda)$  is the reflectivity of graphite which can be calculated from the measured optical constants.<sup>9</sup> The spectral variation of the incident light flux and detector response is thus compensated for. The stability of the detector response was checked prior to each scan, and the system geometry was such that measurements and depositions could be carried out without moving the sample. The reflectivity determined using the above equation has to be corrected for the second-order flux from the monochromator which was estimated by Bailey and Quinn<sup>10</sup> from photoemission measurements of the Cu 3d band.

### III. THEORETICAL MODELS

#### A. Extinction model

At sufficiently low coverage the film can be considered as an array of well-separated identical spheres which act as a filter to the incident and reflected light. The wavelength-dependent extinction efficiency of the particles is defined by

$$Q_{\text{ext}} = \frac{C_{\text{ext}}}{G},$$

where  $C_{\text{ext}}$  is the extinction cross section, and  $G$  is the geometrical cross section of the particles. Following Mie,<sup>2</sup>  $Q_{\text{ext}}$  is given by

$$Q_{\text{ext}} = \frac{2}{x^2} \sum_{n=1}^{\infty} (2n+1) \text{Re}(a_n + b_n),$$

where the complex Mie coefficients  $a_n$  and  $b_n$  are given by

$$a_n = \frac{\Psi'_n(y)\Psi_n(x) - \tilde{n}\Psi_n(y)\Psi'_n(x)}{\Psi'_n(y)\zeta_n(x) - \tilde{n}\Psi_n(y)\zeta'_n(x)}$$

and

$$b_n = \frac{\tilde{n}\Psi'_n(y)\Psi_n(x) - \Psi_n(y)\Psi'_n(x)}{\tilde{n}\Psi'_n(y)\zeta_n(x) - \Psi_n(y)\zeta'_n(x)},$$

where  $\tilde{n}$  is the refractive index of the particle material, and  $\psi$  and  $\zeta$  are Riccati-Bessel functions. The function arguments  $x$  and  $y$  are related to the particle radius  $a$  and the wavelength  $\lambda$  by

$$x = \frac{2\pi a}{\lambda} \quad \text{and} \quad y = \tilde{n} \frac{2\pi a}{\lambda}.$$

From  $Q_{\text{ext}}$ , we can define an effective coverage  $c_{\text{eff}}$  by

$$c_{\text{eff}}(\lambda) = c[(1-c^2)Q_{\text{ext}}D + c^2(Q_{\text{ext}}D)^2],$$

where  $D$  is a correction factor to  $Q_{\text{ext}}$ , for the finite aperture of the detector given by Gumprecht and Sliepcevich,<sup>11</sup> and  $c$  is the geometric line-of-sight coverage. The squared term accounts for the proportion of light suffering extinction as it leaves the sample. For an angle of incidence  $\theta$  relative to the sample normal,  $c$  is related to the normal coverage  $c_n$  by

$$c = \frac{c_n}{2} \left[ \tan \left\{ \frac{(90-\theta)}{2} \right\} + \frac{1}{\tan \left\{ \frac{(90-\theta)}{2} \right\}} \right].$$

To calculate the sample reflectivity, we assume that a proportion of the radiation  $c_n/c$ —that is, the light incident on the normal projection of the particles onto the surface—is reflected from a graphite/metal interface, the remainder being reflected from the graphite/vacuum interface. The reflectivity is thus

$$R(\lambda) = [1 - c_{\text{eff}}(\lambda)][c_n R_{12}(\lambda) + (1 - c_n)R_{23}(\lambda)],$$

where  $R_{12}(\lambda)$  and  $R_{23}(\lambda)$  are the reflectivities at the graphite/metal and graphite/vacuum interfaces, respectively. In calculating  $R_{23}(\lambda)$ , the modification of the refractive index of the vacuum just above the sample due to the polarization of the particles is taken into account, introducing a third parameter  $\alpha$ , the polarizability of the particles. This allows some shape dependence to be included despite assuming spherical particles in the calculation of the extinction. For each sample, the parameters  $a$ ,  $c$ , and  $\alpha$  are adjusted to minimize the weighted fit index defined by

$$\chi = \sum \left\{ \left[ \frac{R_m - R_{\text{min}}}{R - R_{\text{min}}} \right] \left[ \frac{R_m - R_c}{R} \right] \right\}^2,$$

where  $R_m$  and  $R_c$  are the measured and calculated reflectivities, respectively, and  $R_{\text{max}}$  and  $R_{\text{min}}$  are the maximum and minimum values of the measured reflectivity. The model gives very good fits to the data for coverages up to a few percent, as shown in Fig. 1(b) for a low-coverage vanadium film. For thicker films there is increasing disagreement with coverage, and the model breaks down either due to the neglect of interactions among the particles or the assumption of spherical particles. The higher-coverage model presented below, which formally includes a shape factor, indicates increasing ellipticity of metal islands with coverage.

#### B. Islanded film model

An alternative approach to calculating the reflectivity is to consider the overlayer as a continuous film with an effective refractive index corresponding to an inhomogeneous medium. Maxwell-Garnett<sup>5</sup> treated the discontinuous medium as a dispersion of small metal spheres, and used the Clausius-Mosotti equation to obtain the effective dielectric constant of the film in terms of the dielectric constant of the bulk material. Subsequent improvements in the model included generalizing the shape of the particles to ellipsoids of revolution,<sup>12</sup> and considering the interactions between the particles to be of the same form as between static dipoles.<sup>13</sup> Jarrett and Ward incorporated these improvements to model the absorption of visible light by discontinuous gold and silver films. They showed that the effective dielectric constants of the film are given by

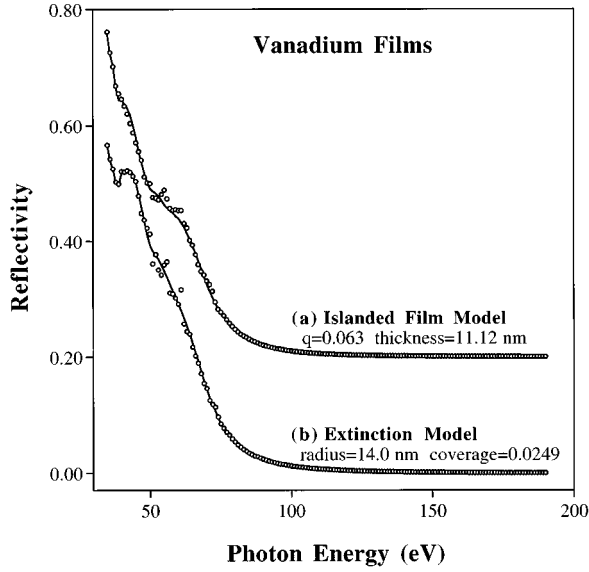


FIG. 1. (a) Comparison of measured and calculated reflectivity, using the islanded film model of an intermediate coverage vanadium film showing the values of film thickness and volume filling fraction ( $q$ ) giving the optimum fit to the data. (b) Comparison of measured and calculated reflectivity, using the extinction model, of a low coverage vanadium film showing the values of particle radius and coverage giving the optimum fit. (○) Measured reflectivity. (—) Calculated reflectivity.

$$\epsilon'_1 = \frac{\epsilon_a \{1 + q[\epsilon_1 \epsilon_a (1 - 2F) + F(\epsilon_1^2 + \epsilon_2^2) - \epsilon_a^2 (1 - F)]\}}{[\epsilon_a + F(\epsilon_1 - \epsilon_a)]^2 + (F\epsilon_2)^2}$$

and

$$\epsilon'_2 = \frac{q\epsilon_2\epsilon_a^2}{[\epsilon_a + F(\epsilon_1 - \epsilon_a)]^2 + (F\epsilon_2)^2},$$

where  $\epsilon_1$  and  $\epsilon_2$  are the dielectric constants of the bulk material,  $\epsilon_a$  is the dielectric constant of the medium in which the particles are embedded,  $q$  is the volume filling fraction of the film, and  $F$  is a shape factor given by

$$F = f(1 - q),$$

where  $f$  is the shape factor introduced by David,<sup>12</sup> and whose components parallel and perpendicular to the plane of the substrate are given by

$$f_{\parallel} = \frac{1}{2} w (w^2 + 1) \left[ \frac{1}{2} \pi - \tan^{-1} w - \left( \frac{w}{w^2 + 1} \right) \right]$$

and

$$f_{\perp} = 1 - 2f_{\parallel}.$$

Here  $w$  is related to the ratio of the half axes,  $a$  and  $b$  of the ellipsoids, by

$$w = \frac{1}{b^2/a^2 - 1}.$$

Having calculated the effective refractive index of the film, the reflectivity of the sample can be calculated as a function of the film thickness  $d$ , and the fit index minimized as a

function of the parameters  $q$ ,  $d$ , and  $b/a$ . The shape parameter is the least significant of these, producing only marginal improvements over a two-parameter fit using just  $q$  and  $d$ , and assuming spherical particles. It does, however, show consistent trends with coverage, and is included in the data presented below.

There is some debate about the appropriate value to use for  $\epsilon_a$ . Jarrett and Ward found that the best fit to their data was obtained using the real part of the dielectric constant of the substrate material, whereas in the present work we obtain the best fits using  $\epsilon_a = 1$ . This may be due to the large difference in wavelengths used. Figure 1(a) shows a comparison between the measured reflectivity and a calculation using this model for an intermediate coverage vanadium film, and demonstrates the good agreement obtainable. The model works well up to  $q$  values of about 0.6, but then shows increasingly poor agreement with experiment. This is probably due to the formation of a continuous conducting network in the film above the percolation threshold. At very low coverage it gives good agreement, but the extinction model does slightly better.

### C. Optical constants

Both models require the bulk refractive index, i.e.,  $n$  and  $k$ , of graphite and the metal overlayers in the xuv region. The data for chromium was obtained mainly from Palik,<sup>14</sup> which reports values in the range 0.04–10 keV. There is a gap in the data for  $n$  in the range 29.5–51.5 eV, but these values can be found using a Kramers-Kronig integral of  $k$  for which there is a complete set of data. In the same Ref. 14 are published values of  $n$  and  $k$  for vanadium up to 120 and 300 eV, respectively. In the region between 120 and 200 eV there are no vanadium absorption edges, so the  $n$  values in this range were approximated by a plasmon tail function. Data for graphite over the whole spectral range is reported by Hagemann, Gudat, and Kunz.<sup>9</sup> Manganese  $k$  values in the range 40–300 eV can be calculated from the optical-absorption measurements reported by Sonntag, Haensel, and Kunz,<sup>15</sup> but there are no measurements of  $n$  available above 20 eV.<sup>16</sup> Atomic cross-section ( $f1, f2$ ) tables<sup>17</sup> were used to calculate values above 50 eV for which  $f1$  values are available. The gap between 20 and 50 eV was filled by a Kramers-Kronig integral of  $k$  for which values over a wide photon energy range can be obtained by combining the data of Johnson and Christy<sup>18</sup> (0.64–6.6 eV), Girouard and Van Truong<sup>16</sup> (6–20 eV),  $f2$  values from Ref. 17 (20–40 eV), Sonntag, Haensel, and Kunz<sup>15</sup> (40–297 eV), and  $f2$  values from Ref. 17 (297–5997 eV). There is good agreement in the  $k$  values in regions where overlap occurs between different sources; however, in the results for manganese presented in Sec. IV C it is clear that there is a discrepancy of about 5 eV, in the position of the feature due to the  $M_{II,III}$  absorption edge at around 50 eV between the calculated and measured reflectivities. In this region,  $k$  values were calculated from the  $f2$  values reported in Ref. 17, so our data indicate a slight error in the position of the edge in this table.

## IV. RESULTS

### A. Chromium

Figure 2 shows the spectral dependence of the reflectivities of several chromium films grown with the substrate at

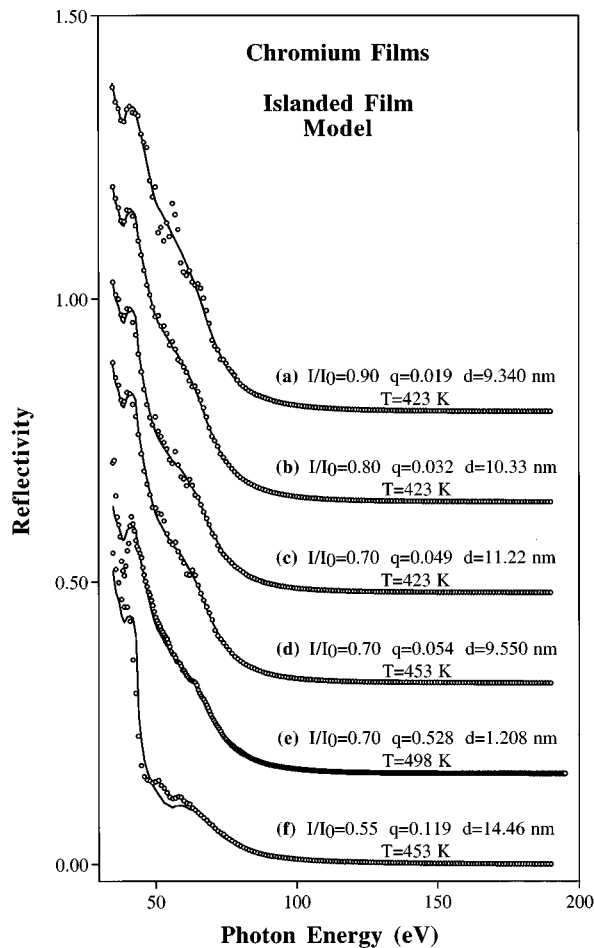


FIG. 2. Measured and calculated reflectivities, using the islanded film model, of various coverage chromium films grown at different substrate temperatures showing the values of film thickness ( $d$ ) and volume filling fraction ( $q$ ) giving the optimum fit to the data. The  $I/I_0$  ratio is the attenuation of the clean graphite reflectivity at a photon energy of 81.5 eV. (○) Measured reflectivity. (—) Calculated reflectivity.

three different temperatures. The fitted curves were all calculated using the islanded film model, and values of the volume filling fraction and film thickness giving the optimum fit to the data are displayed. Figure 3 shows the reflectivity as a function of evaporation time of chromium films deposited with the substrate at two different temperatures. The reflectivity shows oscillations due to interference as the optical thickness grows. This is shown more clearly below for the manganese films where the evaporation rate was sufficiently high to record the reflectivity up to higher thicknesses, and go beyond the first oscillation.

The absolute value of the reflectivity at the minimum is given by the islanded film model for a unique combination of  $q$  and  $d$ , so the curves in Fig. 3 can each yield an extra datum in a plot of  $q$  and  $d$  versus coverage. This involves making an assumption about the particle shape, but the results presented below show that for all three materials, the islands are approximately spherical at coverages around the first reflectivity minimum.

The product of the  $q$  and  $d$  values emerging from the islanded film model is proportional to the total amount of

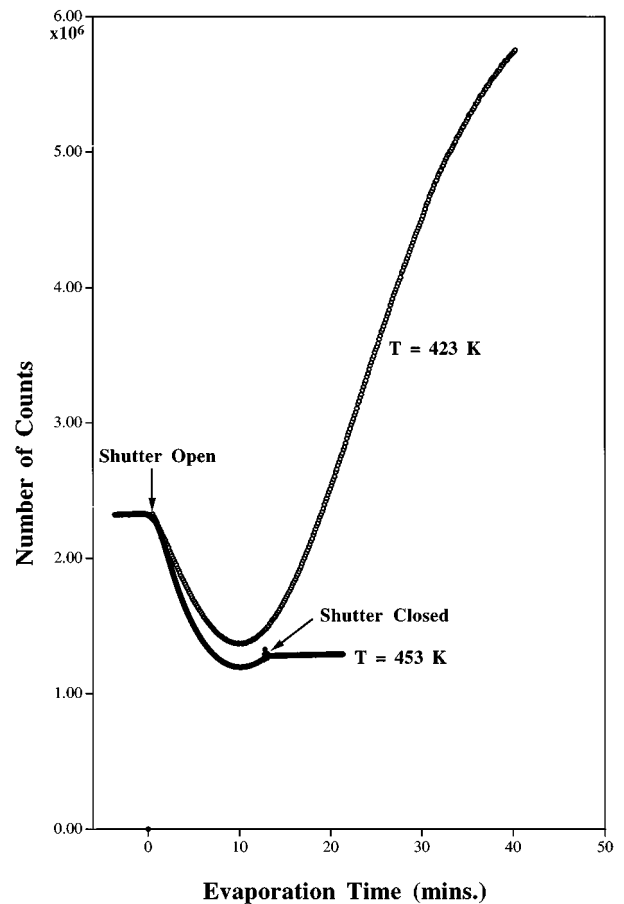


FIG. 3. Reflectivity of chromium films grown with the substrate at two different temperatures, at a photon energy of 81.5 eV, as a function of evaporation time.

material in the film. It is plotted in Fig. 4 for all samples as a function of evaporation time normalized to the time at the first reflectivity minimum. The linear relationship indicates that the sticking probability is constant as a function of coverage and temperature in the range 423–498 K. From now on parameters will be plotted against the product  $qd$  to display variation as a function of coverage.

Figures 5 and 6 show the variation of the volume filling factor and the film thickness with coverage, respectively, for films grown with the substrate at 423 and 453 K. Also shown are least-squares power-law fits to the data points. At the lower temperature the film thickness rapidly grows to about 10 nm and thereafter stays almost constant, whereas heating the substrate a further 30° results in a thickness variation closely following a (coverage)<sup>1/3</sup> dependence. The variation of the volume filling factor with coverage is close to linear, and (coverage)<sup>2/3</sup> dependences at 423 and 453 K, respectively. Both of these results are consistent with simple growth models. A film growing such that:

$$d = \text{const}$$

and

$$q \propto \text{coverage}$$

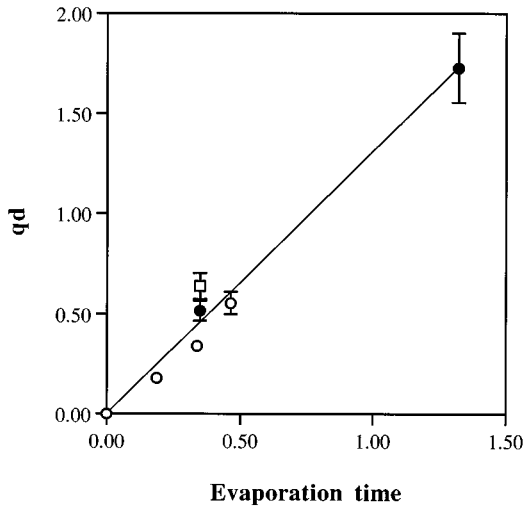


FIG. 4. The product  $qd$  (proportional to the total amount of material in the film) of chromium films as a function of evaporation time normalized to the time at the first reflectivity minimum for all films. (○) Films grown at 423 K. (●) Films grown at 453 K. (□) Films grown at 498 K. (—) Linear fit to all data.

corresponds to islands of constant size increasing in number with evaporation time and a film growing such that

$$d \propto (\text{coverage})^{1/3}$$

and

$$q \propto (\text{coverage})^{2/3}$$

have a constant number of islands whose volume is proportional to evaporation time.

The variation in the ellipticity of the particles as a function of coverage is plotted in Fig. 7 and shows that the islands are close to spherical at low coverage, becoming flatter

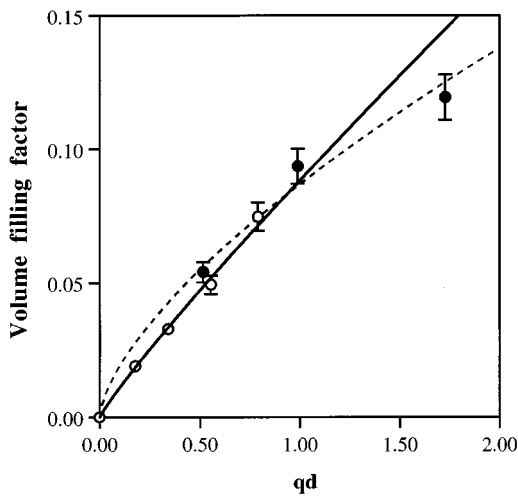


FIG. 5. Volume filling factor of chromium films grown at 423 and 453 K as a function of coverage ( $qd$ ). (○) Films grown at 423 K. (●) Films grown at 453 K. (—) Power-law fit to the data at 423 K [ $q = 0.088(qd)^{0.902}$ ]. (-----) Power-law fit to the data at 453 K [ $q = 0.087(qd)^{0.662}$ ].

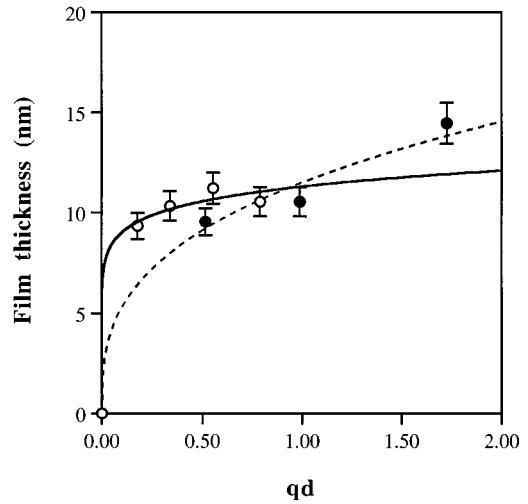


FIG. 6. Film thickness of chromium films grown at 423 and 453 K as a function of coverage ( $qd$ ). (○) Films grown at 423 K. (●) Films grown at 453 K. (—) Power-law fit to the data at 423 K [ $q = 11.302(qd)^{0.098}$ ]. (-----) Power-law fit to the data at 423 K [ $q = 11.500(qd)^{0.338}$ ].

as the film grows. This finding is consistent with that of Jarrett and Ward<sup>3</sup> for gold and silver films on glass and mica substrates.

Figure 8 shows the variation of the volume filling factor and thickness as a function of temperature for three films of approximately the same coverage. Between 453 and 498 K, there is a drastic change in the growth mode with the film grown at the highest temperature consisting of a high density ( $q = 53\%$ ) of small islands with an average size of 1.2 nm. The ratio of major to minor axes vs temperature is plotted in Fig. 9. The trend is to increased oblateness, and the ellipticity parameter for the high-temperature film is greater than 1, indicating a columnar structure. Only one film was grown at 498 K, so the variation of parameters with coverage at this temperature is unknown.

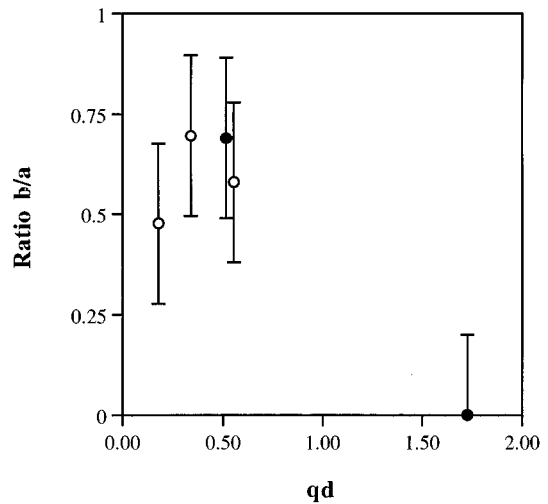


FIG. 7. Ratio of semimajor to semiminor axes as a function of coverage ( $qd$ ) of chromium films. (○) Films grown at 423 K. (●) Films grown at 453 K.

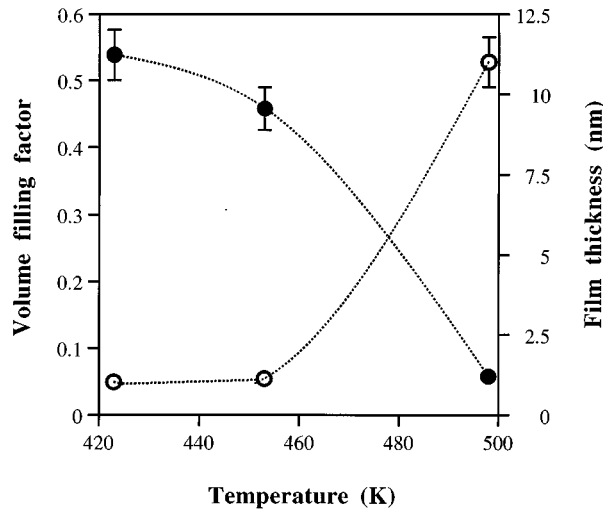


FIG. 8. Volume filling factor and film thickness of similar coverage films as a function of temperature. (○) Volume filling factor. (●) Film thickness.

### B. Vanadium

The spectral dependence of the reflectivity of four vanadium films of different coverages grown with the substrate at 423 K is shown in Fig. 10. Also shown is the calculated reflectivity using the islanded film model and the volume filling factor and film thickness producing the optimum fit. Figure 11 shows the variation of volume filling factor and film thickness with coverage, given by the product of  $q$  and  $d$  determined from the fits using the islanded film model. The two lowest coverage films were also fitted using the extinction model, and  $q$  and  $d$  parameter values corresponding to the particle radius and line-of-sight coverage parameters emerging from the model are shown. A complication in making comparisons like this between models is that the extinction model assumes spherical particles, while the islanded film model explicitly includes a shape parameter. It is there-

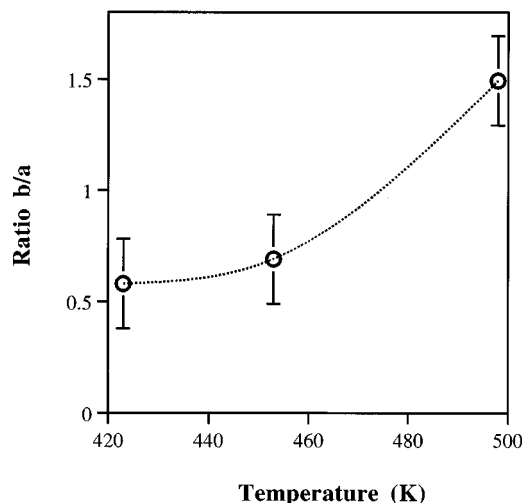


FIG. 9. Ratio of semimajor to semiminor axes of similar coverage films as a function of temperature.

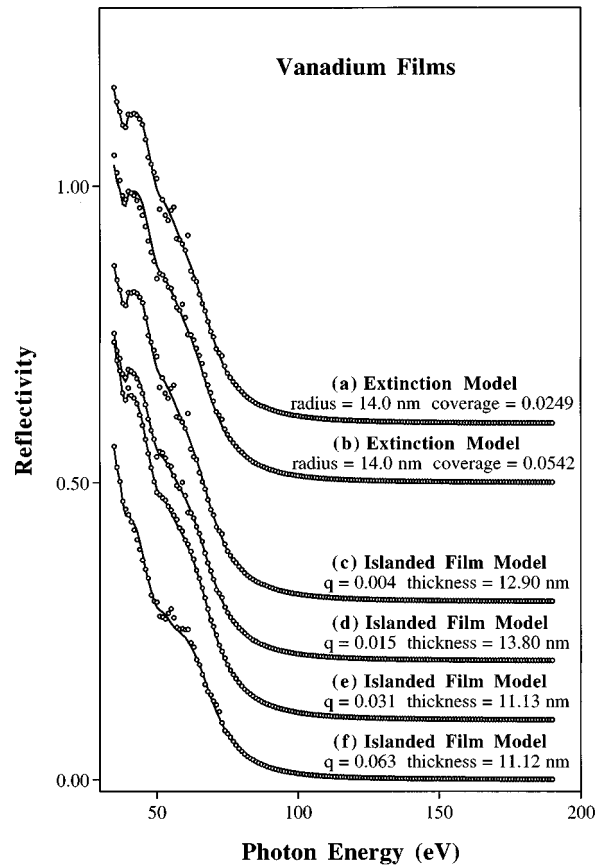


FIG. 10. Measured (○) and calculated (—) reflectivities, of various coverage (specified by  $I/I_0$ —the attenuation of the clean graphite reflectivity at 81.5 eV) vanadium films. (a) and (b) Low coverage films fitted using the extinction model showing values of particle radius and film coverage giving the optimum fit. (c)–(f) Films fitted using the islanded film model showing values of film thickness ( $d$ ) and volume filling fraction ( $q$ ) giving the optimum fit.

fore assumed that the particle radius given by the extinction model corresponds to the average of the major and minor axes of the ellipsoids given by the islanded film model. Due to the large noise inherent in the shape parameter, this gives a correspondingly large variation in the film thickness evaluated from the extinction model radius parameter as seen in Fig. 11. The volume filling factor corresponding to the line-of-sight coverage given by the extinction model is much less sensitive to island shape, and varies between  $2c_n/3$  and  $c_n$ , where  $c_n$ , the normal coverage is related to the line-of-sight coverage by the geometric factor given in Sec. III. Thus Fig. 11 shows reasonable agreement in the volume filling factor predicted by the two models.

The volume filling factor varies linearly with coverage and the thickness is almost constant. The growth mode is therefore the same as for chromium films at 423 K, that is, constant size islands with increasing density are produced by nucleation of additional islands. It is interesting to note that the average size is similar to that for chromium films. Figure 12 shows the variation of the ellipticity with coverage, and again the trend is the same as for chromium, with the islands becoming flatter as the film density increases.

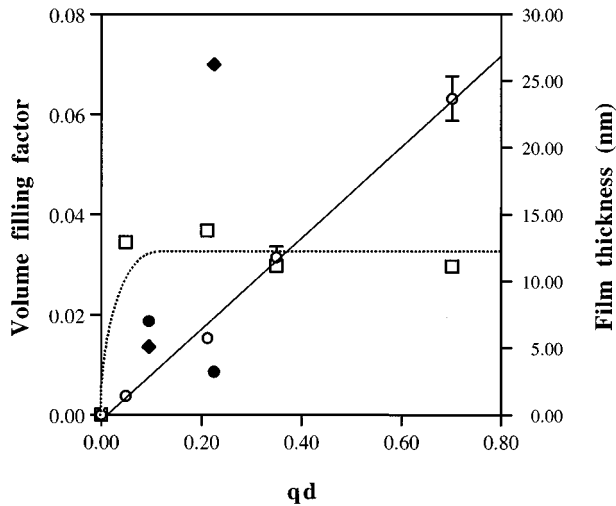


FIG. 11. Volume filling factor ( $q$ ) and thickness ( $d$ ) of vanadium films grown at 423 K as a function of coverage ( $qd$ ) ( $\circ$ )  $q$  values obtained using the islanded film model. ( $\bullet$ )  $q$  values obtained using the extinction model. (—) Linear fit to the  $q$  values obtained using the islanded film model. (---) Values obtained using the islanded film model. ( $\blacklozenge$ ) Values obtained using the extinction model.

### C. Manganese

Figure 13 shows the measured reflectivity at 97 eV of a manganese film, grown with the substrate at 423 K, as a function of evaporation time, demonstrating oscillation as the optical thickness of the film increases. A set of spectral scans is shown in Fig. 14 along with fitted curves using the islanded film model and the volume filling factor ( $q$ ) and film thickness ( $d$ ) values giving the optimum fit. For clarity, not all curves are shown. With increasing coverage the fits become poorer, and it is clear that the reason for this is the discrepancy in the position of the Mn  $M_{II,III}$  absorption feature at about 50 eV between measured and calculated spectra. This was discussed in Sec. III, and we believe it is a

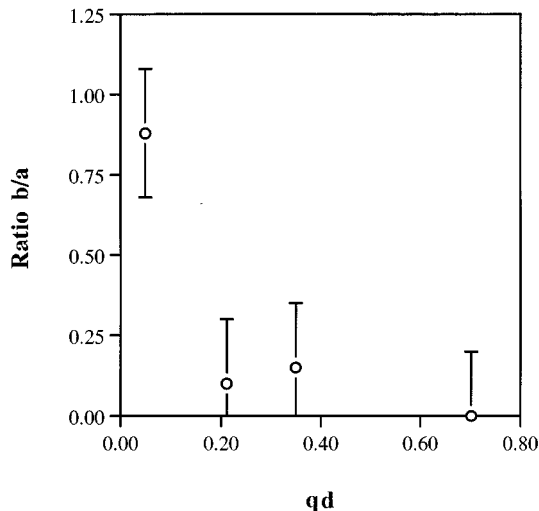


FIG. 12. Ratio of semimajor to semiminor axes as a function of coverage ( $qd$ ) of vanadium films grown at 423 K.

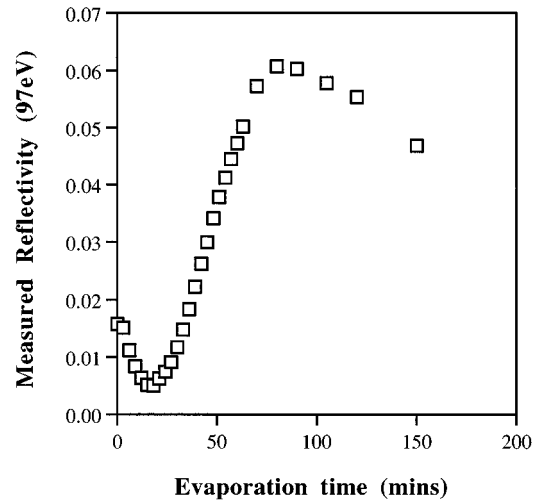


FIG. 13. Reflectivity at 97 eV of the manganese film grown at 423 K as a function of evaporation time.

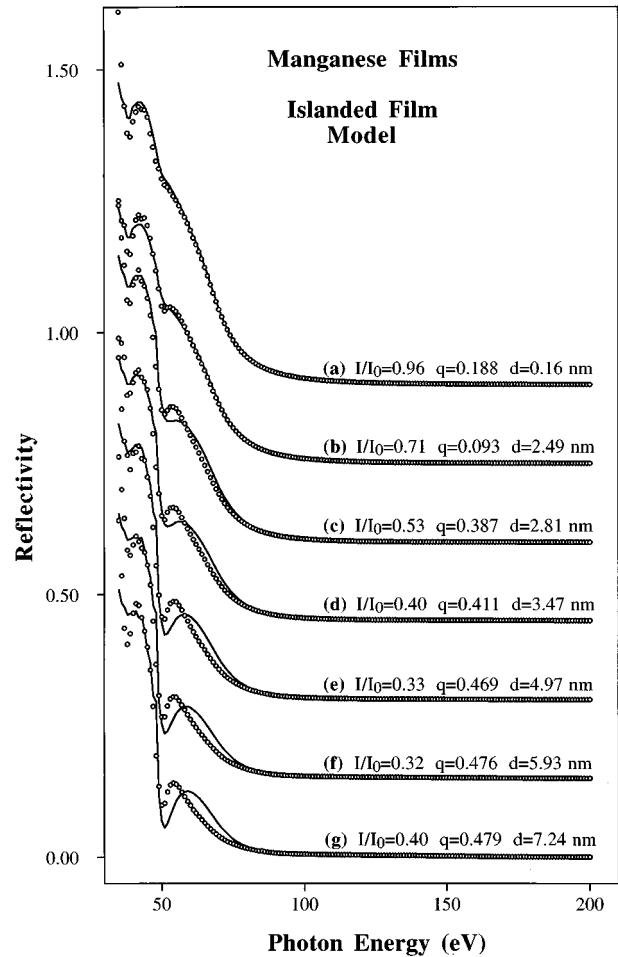


FIG. 14. Measured ( $\circ$ ) and calculated (—) reflectivities, of various coverage (specified by  $I/I_0$ —the attenuation of the clean graphite reflectivity at 97 eV) manganese films showing values of film thickness ( $d$ ) and volume filling fraction ( $q$ ) giving the optimum fit.

result of a small discrepancy in the edge position in the published values of atomic cross sections<sup>17</sup> from which the manganese refractive index was calculated. Despite this, it is apparent that the optimized fit would remain optimized if the feature was shifted to the correct place. We are reasonably confident therefore that the trend in the  $q$  and  $d$  parameters with coverage is reliable.

The  $qd$  product representing the total amount of material on the surface is plotted as a function of evaporation time in Fig. 15. There is clearly a change in sticking probability at about 25 min which correlates with a change in the growth mode of the film demonstrated by the data in Fig. 16, which shows the volume filling factor and film thickness as a function of coverage ( $qd$ ). At the early stages of film growth there is a rapid increase in  $q$  up to nearly 0.5, showing that the film covers large areas of the surface. There then follows a range of coverage where the volume filling factor is constant but the film thickness increases linearly. This can be explained by a vertical columnar growth. At a thickness of about 10 nm, the columns stop increasing in height and grow laterally, as shown by the flattening of the thickness curve and the increase in  $q$ . According to the data in Fig. 15, there is a lower sticking probability for the latter growth mode.

The evolution of the shape of the islands shown in Fig. 17 is consistent with this result. In the initial stages of growth as the film spreads to cover, the surface the islands are flat. The columnar growth corresponds to the steady rise of the island height/diameter ratio till they are about equal followed by a decrease indicating the lateral growth at high coverage.

## V. DISCUSSION

The growth modes determined for the three overlayers are summarized in Table I. The size and shape of a metal island in a growing film is determined by the relative magnitude of the flux of atoms onto the island: from atoms diffusing across the surface and directly from the source and flux off the

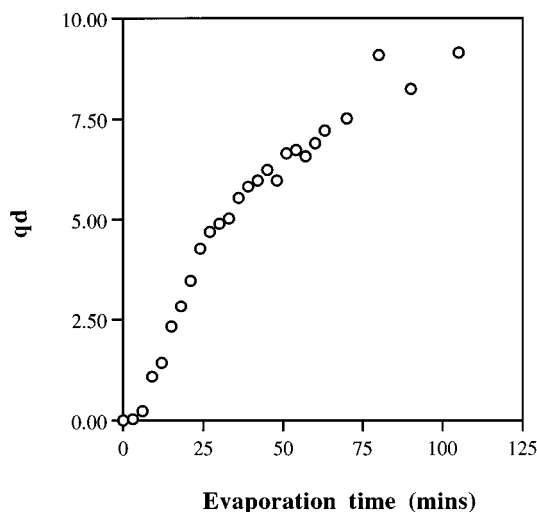


FIG. 15. The product  $qd$  (proportional to the total amount of material in the film) of manganese films as a function of evaporation time. A change in sticking probability is indicated by the vertical line.

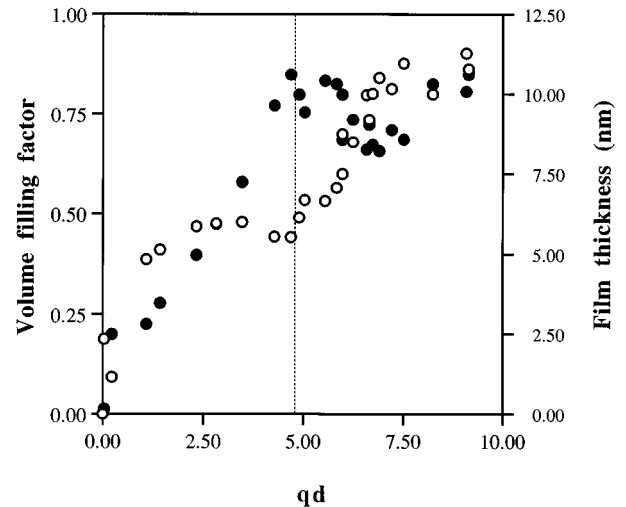


FIG. 16. Volume filling factor (○) and thickness (●) of manganese films grown at 423 K as a function of coverage ( $qd$ ).

island by evaporation. In the case of chromium and vanadium films grown at 423 K, the constant island size indicates a balance of fluxes. Both these materials form layers with a low volume filling fraction, so the flux onto the islands is likely to be dominated by atoms diffusing across the substrate surface. The rate of impingement onto the islands will scale as the linear dimension, whereas the flux off will be related to the area so there will be growth until the two balance. This happens for an average island size around 13 nm in both cases.

Increasing the temperature to 453 K for growing chromium films produces a dominant incident flux by increased diffusion over the graphite surface. The islands in the densest films studied were still growing, and the cube root power-law dependence of size on evaporation time shows that the volume is proportional to time, which indicates a constant imbalance of fluxes. This would be the case if the incident rate

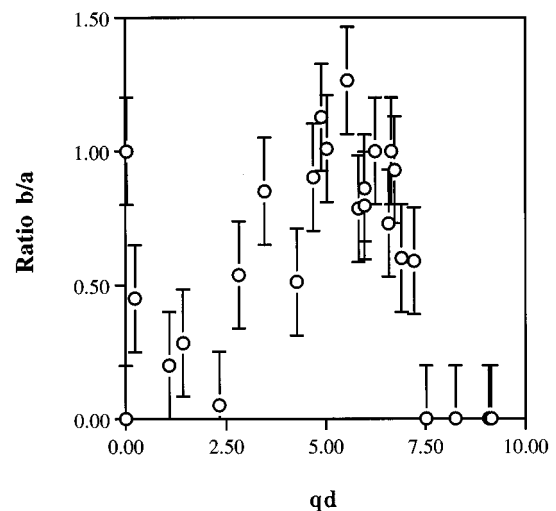


FIG. 17. Ratio of semimajor to semiminor axes as a function of coverage ( $qd$ ) of manganese films grown at 423 K.

TABLE I. Growth modes determined for the three overlayers.

Material	$T=423$ K	$T=453$ K	$T=498$ K
Chromium	Constant size islands $\langle d \rangle = 12.8$ nm growth by nucleation of new islands $q \propto t$ $d = \text{const}$	Constant number of islands growing in size $q \propto t^{2/3}$ $d \propto t^{1/3}$	Dense layer of very small islands $\langle d \rangle = 1.0$ nm
Vanadium	Constant size islands $\langle d \rangle = 12.9$ nm growth by nucleation of new islands $q \propto t$ $d = \text{const}$		
Manganese	Initially forms high coverage layer, followed by vertical growth where $q = \text{constant}$ and $d \propto t$ When island height $\approx$ width, lateral growth occurs where $q \propto t$ and $d = \text{const}$		

of impingement was always dominant over the evaporated flux. Increasing the temperature further to 498 K produces a marked change in the morphology of chromium films to a dense array of small islands. Only one film was prepared at this temperature, so the evolution with time is unknown, but the result indicates a large increase in the rate of evaporation off the islands.

The growth mode of manganese at 423 K is different from the other two materials. It appears that the growing film rapidly covers a large proportion of the surface and then extends vertically. In this case a high proportion of the incident flux is directly from the source, thus the vertical growth of the film is not unexpected. At a thickness of about 10 nm, the film growth mode changes, with an accompanying change in

sticking probability, to horizontal growth. This is hard to interpret in simplistic terms, but must be due to an increased probability of atoms diffusing off the island surfaces and onto the substrate.

## VI. CONCLUSIONS

Combined with a realistic theoretical model, the measured xuv reflectivity of islanded metal films can give detailed information about their morphology. The technique has been used to study the growth of the transition metals, chromium, vanadium, and manganese on graphite, and to demonstrate the critical effect of temperature on the growth mode of the film.

<sup>1</sup>M. Faraday, *Philos. Trans. R. Soc. London* **147**, 145 (1857).

<sup>2</sup>G. Mie, *Ann. Phys.* **25**, 377 (1908).

<sup>3</sup>D. N. Jarrett and L. Ward, *J. Phys. D* **9**, 1515 (1976).

<sup>4</sup>W. T. McKenna and L. Ward, *Phys. Status Solidi A* **68**, K11 (1981).

<sup>5</sup>J. C. Maxwell-Garnett, *Philos. Trans. R. Soc. London Ser. A* **205**, 237 (1906).

<sup>6</sup>H. Schade and Z. E. Smith, *Appl. Opt.* **24**, 3221 (1985).

<sup>7</sup>C. Binns and S. C. Bayliss, *Surf. Sci.* **214**, 165 (1989).

<sup>8</sup>C. Binns, C. Norris, H. S. Derbyshire, and S. C. Bayliss, in *Physics and Chemistry of Finite Systems: from Clusters to Crystals*, Vol. 374 of *NATO Advanced Study Institute, Series C: Mathematical and Physical Sciences*, edited by X. Jena, X. Khanna, and X. Rao (Kluwer, Dordrecht, 1992).

<sup>9</sup>H.-J. Hagemann, W. Gudat, and C. Kunz (unpublished).

<sup>10</sup>P. Bailey and F. M. Quinn (unpublished).

<sup>11</sup>R. O. Gumprecht and C. M. Sliepcevich, *J. Chem. Phys.* **57**, 90 (1953).

<sup>12</sup>E. David, *Z. Phys.* **114**, 389 (1939).

<sup>13</sup>T. Yamaguchi, S. Yoshida, and A. Kinbara, *Thin Solid Films* **13**, 261 (1972).

<sup>14</sup>E. D. Palik, *Handbook of the Optical Properties of Solids* (Academic, Orlando, 1984).

<sup>15</sup>B. Sonntag, R. Haensel, and C. Kunz, *Solid State Commun.* **7**, 597 (1969).

<sup>16</sup>F. E. Girouard and Vo-Van Truong, *J. Opt. Soc. Am.* **1**, 76 (1984).

<sup>17</sup>B. L. Henke, E. M. Gullikson, and J. C. Davis, *At. Data Nucl. Data Tables* **54**, 181 (1993).

<sup>18</sup>P. B. Johnson and R. W. Christy, *Phys. Rev. B* **9**, 5056 (1974).